Biophysical Chemistry 25 (1986) 253–269
Elsevier



BPC 01109

# DYNAMIC LIGHT-SCATTERING STUDY ON POLYMERIZATION PROCESS OF MUSCLE ACTIN *

Junji MASAI [a,**], Shin'ichi ISHIWATA [b] and Satoru FUJIME [a,***]

[a] *Mitsubishi-Kasei Institute of Life Sciences, Machida, Tokyo 194 and* [b] *Department of Physics, Waseda University, Shinjuku-ku, Tokyo 160, Japan*

Received 4th July 1986
Revised manuscript received 13th September 1986
Accepted 17th October 1986

*Key words: Actin polymerization; Diffusion coefficient; Dynamic light scattering; Spontaneous fragmentation; Quasistationary process*

Globular actin (G-actin) polymerizes into a fibrous form (F-actin) under physiological salt conditions. The polymerization process of muscle actin was studied by a dynamic light-scattering method. The intensity correlation functions $G^2(\tau)$ of scattered light from a G-actin solution containing 2 mM Tris-HCl (pH 8.0) and 0.1 mM ATP were analyzed by a cumulant expansion method, and the translational diffusion coefficient was determined to be $D = (8.07 \pm 0.10) \times 10^{-7}$ cm$^2$/s at 20°C. This $D$ value gave a diameter of 5.3 nm for spherical G-actin including a hydration layer. Polymerization of 1–3 mg/ml G-actin in a solution containing 10 mM Tris-HCl (pH 8.0), 0.2 mM ATP and 60 mM KCl was followed by successive measurements of $G^2(\tau)$ for a data accumulation period of 60–300 s/run. The time evolution of $G^2(\tau)$ was analyzed by a least-squares fitting to the field correlation function of a multiexponential form $g^1(\tau) = \Sigma_i A_i \exp(-\Gamma_i \tau)$ with $\Gamma_1 > \Gamma_2 > \Gamma_3 > \ldots$, and the static scattering intensity $I(t) = \langle I \rangle$ as a function of time $t$ after initiation of polymerization was decomposed as $I(t) = \langle I \rangle \Sigma_i A_i$. At the early stage of polymerization, a two-exponential fit gave results indicating that component 1 came from G-actin and component 2 from F-actin growing linearly with $t$. At the middle stage of polymerization, a three-exponential fit gave the results that component 1 came from G-actin and possibly its small oligomers, component 2 from polymers with a number-average length $L_n$ of about 900 nm which was independent of $t$, and component 3 from 'ghosts' in dynamic light scattering in a semidilute regime. Component 3 was concluded to arise from restricted motions of polymers with lengths much longer than $L_n$ in cages formed by polymers giving component 2, and a fragmentation-elongation process of F-actin was suggested to start at the middle stage of polymerization, resulting in the size redistribution of F-actin.

## 1. Introduction

G-Actin, one of the muscle proteins, is globular in shape and about 6 nm in diameter. G-Actin polymerizes into F-actin (fibrous form) under physiological salt concentrations. Based on observations by electron microscopy, a 'pearl-and-necklace' model is proposed for the ultrastructure of F-actin. F-Actin is a two-stranded helical polymer. The half pitch of the helix is 36 nm and within this length there are 13 G-actins. The polymerization process of actin has been extensively studied by various techniques such as viscometry, flow birefringence, fluorometry, static light scattering, etc. [1,2]. In this paper, the polymerization process of actin was studied by dynamic light scattering, aiming both at a comparison of the present result with previous ones on the one hand,

* Dedicated to Professor F. Oosawa on the occasion of his retirement from Osaka and Nagoya Universities (1986). He pioneered the study of actin polymerization, and has fostered many researchers including all of us.

** Present address: Research Center, Mitsubishi Chemical Industries Ltd., 1000 Kamoshida, Midori-ku, Yokohama 227, Japan.

*** To whom correspondence should be addressed.

and at an application of dynamic light scattering to a 'quasistationary' process on the other. General background information about dynamic light scattering can be found in standard textbooks [3,4].

This work was partially presented in preliminary form at the 1983 meetings of the Physical Society of Japan (March, Abstract no. 29pHJ4) and the Biophysical Society of Japan (October, Abstract no. 2B1445).

## 2. Preliminary consideration of problems

### 2.1. Actin polymerization

To give rough background information concerning the polymerization process of actin, we briefly summarize the pioneering theoretical study on kinetics of actin polymerization by Oosawa and Kasai [5]. Extensive information about the polymerization of actin can be found in a monograph [1] and also a recent review article, for example, ref. 2. In a salt-free solution, actin is in its monomeric form (G-actin). After addition of salt to the G-actin solution, polymerization of G-actin to F-actin commences. The initial process of polymerization consists of nucleation and elongation. A few (probably 2–3) G-actins, the number of which is denoted by $q$, form a special shape (or state) of an aggregate, which acts as a nucleus of polymerization. Let $C_1$ be the number concentration of monomers, $p$ be the number concentration of nuclei (and hence of polymers; spontaneous fragmentation of polymers is omitted here) and $k_+^*$ be the kinetic constant of the forward reaction of the formation of nucleus. Then, we have

$$\mathrm{d}p/\mathrm{d}t = k_+^* C_1^q \quad \text{(nucleation)} \tag{1}$$

Let $C_0$ be the total number concentration of monomers before initiation of polymerization, $C_h$ be the total number concentration of monomers incorporated into all polymers present in solution, $C_0 = C_h + C_1$, and $k_+$ be the kinetic constant of the forward reaction of elongation of polymers. We then have

$$\mathrm{d}C_h/\mathrm{d}t = -\mathrm{d}C_1/\mathrm{d}t = k_+ p C_1 \quad \text{(elongation)} \tag{2}$$

In both eqs. 1 and 2, backward reactions were neglected because we are considering the initial stage of polymerization. Eqs. 1 and 2 can be solved to give simple forms of solutions, $C_1(t) = C_0[\mathrm{sech}(\alpha t)]^{2/q}$ and $p(t) = p(\infty)\tanh(\alpha t)$, where $\mathrm{sech}(z)$ and $\tanh(z)$ are hyperbolic functions, $\alpha^2 = (1/2)qk_+^* k_+ C_0^q$ and $p(\infty)^2 = 2k_+^* C_0^q/(k_+ q)$, or

$$C_h(t) = C_0\{1 - [\mathrm{sech}(\alpha t)]^{2/q}\} \tag{3}$$

$$\langle L(t)\rangle = L_0 C_h(t)/p(t) = \langle L(\infty)\rangle\{1 - [\mathrm{sech}(\alpha t)]^{2/q}\}/\tanh(\alpha t) \tag{4}$$

where $\langle L(t)\rangle$ is the number-average length over all polymers and $L_0$ the subunit length of the polymer. (There is a typographical error in the literature: the factor 2 on the right-hand-side of eq. 48 in ref. 1 and of eq. 21 in ref. 5 should read $2^{1/2}$.) Graphic representations of the time evolution of $p(t)$, $C_h(t)$ and $\langle L(t)\rangle$ are given in fig. 1. Because of the neglect of backward reactions and fragmentation, the above analysis is applied only to the initial stage of polymerization. However,

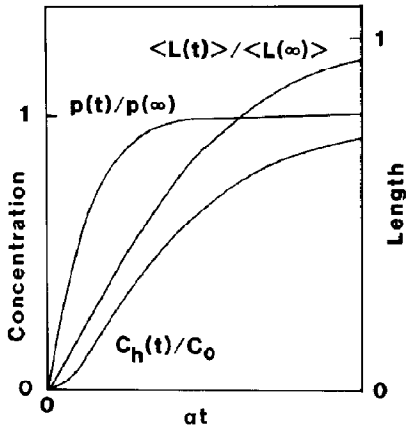


Fig. 1. Theoretical predictions for the early stage of actin polymerization based on the kinetic theory of Oosawa and Kasai [5]. $C_0$ denotes the number concentration of G-actin before initiation of polymerization. $p(t)$ and $C_h(t)$ denote, respectively, the number concentrations of nuclei and G-actin incorporated into all actin filaments at time $t$ after initiation of polymerization. $\langle L(t)\rangle \equiv L_0 C_h(t)/p(t)$ is the number-average length of F-actin, $L_0$ being the subunit length. $q = 3$ was assumed.

the above analysis provides us with important information. (a) At time $t$ when $C_h(t) = C_0/4$, $p(t)$ already becomes about 80% of $p(\infty)$; the nucleation process finishes at an early stage of polymerization. Due to this, the length distribution of polymers is of a Poisson type at the early stage of polymerization. (b) At the initial stage of polymerization, the average length of polymers increases linearly with $t$.

In the middle and later stages of polymerization, the main processes are of elongation and size redistribution of F-actin, which result in a final length distribution of exponential form, $\exp(-L/\langle L\rangle)$.

### 2.2. Light scattering

The number $n(t)$ of photoelectron pulses in a digital method is recorded with a sampling time $\Delta\tau$ (in s). Then, we have sampled values of $n(t)$ such as $n(t, \Delta\tau)$, $n(t+\Delta\tau, \Delta\tau), \ldots, n(t+m\Delta\tau, \Delta\tau), \ldots$, where $n(t+m\Delta\tau, \Delta\tau)$ is the total counts of photons of scattered light measured over the time interval $[t+m\Delta\tau, t+(m+1)\Delta\tau]$, which is simply written as $n(m\Delta\tau)$. The average counts of photons per sampling time over a long time $T$ is defined by $\langle n\rangle = \sum_m n(m\Delta\tau)/N$, where $N = T/(\Delta\tau)$ is the total number of samples of $n(m\Delta\tau)$. The normalized intensity correlation function is given by $g^2(\tau) = \langle n(0)n(m\Delta\tau)\rangle/(\langle n\rangle^2 N) = |g^1(\tau)|^2 + 1$, where $\tau = m\Delta\tau$ $(m = 1, 2, \ldots, M)$ and $g^1(\tau)$ is the normalized field correlation function of scattered light. Measurements of $g^2(\tau)$ by use of a dedicated computer (or a digital correlator) give us information about the statistical nature of the scattered light field and hence the statistical behavior of the scatterer with time. From an experimental point of view, unnormalized forms of relevant expressions are more suitable. The total counts of photoelectrons during the time interval from 0 to $T$ is given by

$$\langle I\rangle = N\langle n\rangle = \sum_m n(m\Delta\tau) \tag{5}$$

and the unnormalized intensity correlation function by

$$G^2(\tau) = (\langle I\rangle^2/N)\left[|g^1(\tau)|^2 + 1\right] \tag{6}$$

Let us consider the Brownian motion of large scatterers (solute molecules) compared with solvent molecules. The intensity $I(t)$ at time $t$ of scattered light from such a system fluctuates, the fluctuation being characterized by time $\tau_B$ (the correlation time of the Brownian motion of the scatterer). Then, if we want to measure the average intensity $\langle I\rangle$ of scattered light, for example, with 1% accuracy, we need a measuring (averaging) time $\tau_E$ of the order of $10^4$-times longer than $\tau_B$. If such quantities as sizes and/or size distribution of scatterers, for example, evolve with time as discussed in this paper, we have another measure of time $\tau_s$ characteristic of the time evolution of the system ($\tau_s = 1/\alpha$ in a particular example given in eqs. 3 and 4). If $\tau_s \gg \tau_E \gg \tau_B$, the system is said to be in a stationary state from the viewpoint that the time evolution of the system is very slow compared with the measurements of various statistically averaged quantities of scattered light such as $\langle I\rangle$ and $G^2(\tau)$. If $\tau_s > \tau_E \gg \tau_B$, the system is said to be in a quasistationary state from the viewpoint that it is possible to follow the time evolution of the system by measuring various statistically averaged quantities of scattered light in spite of a rather rapid change in the system. If $\tau_s$ is close to $\tau_E$ or $\tau_s < \tau_E$, any statistically averaged quantity is no longer measurable and the system is said to be in a transient state.

Another problem is as follows. If we set $\Delta\tau \ll \tau_B$, we can follow the fluctuations in the intensity of scattered light due to the Brownian motion of the scatterers. However, if we set $\Delta\tau$ too short, the number of photons $n(m\Delta\tau)$ becomes so small that in order to obtain $G^2(\tau)$ with reasonable accuracy, we need a measuring time much longer than $\tau_E$. For example, if $\tau_B = 100$ μs, we may need $\tau_E = 1$ s. If the intensity of scattered light is $10^4$ counts/s, we have the average intensity (the total counts) $\langle I\rangle = N\langle n\rangle = 10^4$ counts for $\tau_E = 1$ s, and hence the statistical accuracy in $\langle I\rangle$ is $(10^4)^{1/2}/10^4 = 1\%$. In this particular example, if we set $\Delta\tau = 5$ μs, $\langle n\rangle$ is only $5\times10^{-2}$ counts. Then, we have $G^2(\infty) = \langle I\rangle^2/N = \langle n\rangle^2 N = 500$. The measurement of $G^2(\tau)$ for $\tau_E = 1$ s results in only 4.5% statistical accuracy. To attain 1% accuracy in $G^2(\tau)$, $\tau_E = 20$ s will be required. Namely, as far as $\tau_s \gg \tau_E$ high accuracy in $G^2(\tau)$ will be

obtained by simply lengthening $\tau_E$, but when $\tau_s$ approaches $\tau_E$ the situation is not so simple.

The remainder of this paper describes the study on the polymerization process of actin as an example of the applications of the dynamic light-scattering technique to the study of quasistationary processes. Some previous examples of this kind of application to biological and related subjects have been reviewed by Cummins [6].

## 3. Materials and methods

### 3.1. Materials

G-Actin from rabbit back and leg muscle was prepared and purified by standard methods: dry muscle was prepared by almost the same method as that of Straub [7], except that the regulatory proteins were removed before acetone treatment of myosin-extracted minced muscle [8]. G-Actin was purified according to the method of Spudich and Watt [9] with slight modifications. In the final step of purification, F-actin was dialyzed for 72 h against 2 mM Tris-HCl and 0.1 mM ATP at pH 8.0 (preparation a), and against 2 mM Tris-HCl, 0.1 mM ATP and 0.2 mM $CaCl_2$ at pH 8.0 (preparation b). Preliminary examinations of the G-F transformation were made each day for both preparations of G-actin by use of an Ostwald viscometer. For each preparation, the time course of the increase in viscosity at 20°C after initiation of polymerization by 60 mM KCl was the same within experimental errors up to at least 3 days. 4 days after dialysis, a small decrease in the rate of polymerization was observed in preparation a but not in b. The saturation value of the solution viscosity was the same for both preparations of G-actin 4 days after dialysis, suggesting no appreciable degradation in polymerizability of metal-free G-actin. G-Actin was less stable and the rate of polymerization was faster in preparation a than in b. In the following experiments, therefore, we used G-actin in preparation a stored on ice, and measurements were made within 3 days in the presence and absence of added $CaCl_2$. No measurements were made in the presence of $MgCl_2$.

A solution of an appropriate concentration of G-actin in a suitable amount of Tris-HCl buffer (pH 8.0) and ATP was filtered by a membrane filter with pore size 25 nm (Nippon Millipore, Tokyo) directly into a 10 mm outer diameter cylindrical scattering cell, which had been thoroughly rinsed with the filtered buffer solution. The G-actin solution in the scattering cell was then centrifuged at 4°C and at $20000 \times g$ for more than 12 h. This centrifugation was essential in obtaining reliable correlation functions for G-actin. After several measurements for G-actin, polymerization of actin in the cell was initiated by adding a drop of 0.5 M KCl solution from an injection needle attached to a filter device and carefully tilting the cell several times to allow the solution to flow in the cell for rapid mixing, which resulted in a final salt concentration of $(60 \pm 2)$ mM KCl with virtually no dilution of other components. This procedure gave a reproducible time course of the change in the static scattering intensity run by run, and mixing was concluded to be quite satisfactory. The time $t$ after initiation of polymerization counted not from the moment of the addition of a drop of the salt solution but from the moment of last tilting of the cell, so that there was ambiguity in the zero point of $t$ by about 10 s. At $t = 2$ min, measurements of correlation functions started. For each preparation of G-actin from acetone powder, we usually made two runs of dynamic light-scattering measurements for a given experimental condition, just after and 1 or 2 days after the final dialysis. There was no appreciable difference in the results in these two runs.

### 3.2. Dynamic light scattering

Dynamic light-scattering measurements were carried out by using a conventional apparatus described elsewhere [10]. The intensity autocorrelation function $G^2(\tau)$ can be written as (cf. eq. 6)

$$G^2(\tau) = B\left[\beta\,|\,g^1(\tau)\,|^2 + 1\right] \tag{7}$$

where $\tau = m\Delta\tau$ ($m$, channel number; $\Delta\tau$, channel width or sampling time of the digital correlator), $B$ is the baseline level ($B^{1/2}$ is proportional to the static scattering intensity $\langle I \rangle$, see eq. 6) and $\beta$ a machine constant. For a globular scatterer, $g^1(\tau)$

has a simple form of $g^1(\tau) = \exp(-\Gamma\tau)$, where $\Gamma = DK^2$, $D$ being the translational diffusion coefficient of the scatterer and $K$ the length of the scattering vector. Generally speaking, however, the actual $g^1(\tau)$ is not completely singly exponential. Then, a cumulant expansion is applied [11];

$$g^1(\tau) = \exp(-\bar{\Gamma}\tau)\left[1 + (\mu_2/2!)\tau^2 - (\mu_3/3!)\tau^3\right] \quad (8)$$

where $\bar{\Gamma}$ is the average decay rate or the first cumulant of, and $\mu_i$ the $i$-th cumulant of $g^1(\tau)$. In some cases, as in our case described below, a multiexponential fit is useful;

$$g^1(\tau) = \sum_i A_i \exp(-\Gamma_i\tau) \quad (9)$$

where $\Sigma_i A_i = 1.0$ and $\Gamma_1 > \Gamma_2 > \Gamma_3 > \ldots$. An algorithm for a least-squares multiexponential fit is described in appendix A1.

To follow the polymerization process of actin, $G^2(\tau)$ was successively measured after initiation of polymerization. The data accumulation period ($\tau_E$) was 60–300 s/run and between two successive runs there was a dead time of 3 s for data processing.

## 4. Results

### 4.1. Characterization of G-actin

We first measured $G^2(\tau)$ at 5°C for a 3.3 mg/ml G-actin solution in 2 mM Tris-HCl (pH 8.0) and 0.1 mM ATP. The result of the cumulant analysis is depicted in fig. 2, which gave $D = (8.07 \pm 0.10) \times 10^{-7}$ cm$^2$/s at 20°C. The values of $\mu_2/\bar{\Gamma}^2$ were 0.05–0.1 except for the lowest $K^2$ where a slight contribution from dusts was observed. Neither the measurement of the concentration dependence of $D$ nor correction as in ref. 12 was made. This $D$ value is very close to $D^{20,W} = (7.92 \pm 0.07) \times 10^{-7}$ cm$^2$/s (extrapolated to infinite dilution) and about $8.15 \times 10^{-7}$ cm$^2$/s (at 3.3 mg/ml G-actin) [12,13] but distinctly larger than $D^{20,W} = (7.15 \pm 0.35) \times 10^{-7}$ cm$^2$/s (an average for 0.4, 0.8 and 1.6 mg/ml G-actin) [14]. All of these $D$ values, however, are consistent with the size of the monomeric form of actin; if a spherical form is assumed, our $D$ value gives 5.3 nm for the diameter of G-actin including a hydration layer. This result confirmed that G-actin in our preparation was indeed in its monomeric form.

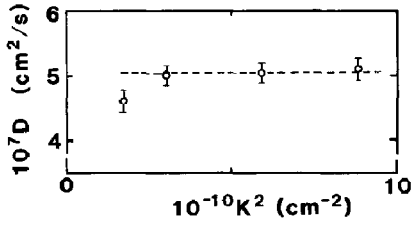


Fig. 2. The $D$ vs. $K^2$ relationship for a 3.3 mg/ml G-actin solution in 2 mM Tris-HCl (pH 8.0) and 0.1 mM ATP at 5°C. Five to ten data were averaged for each $K$ value. From the $D$ value at 5°C we obtained $D = (8.07 \pm 0.10) \times 10^{-7}$ cm$^2$/s at 20°C after $T/\eta$ correction, $T$ being the absolute temperature and $\eta$ the solvent viscosity.

### 4.2. Polymerization of actin under various conditions

We now consider the polymerization process of actin under various conditions. Fig. 3 depicts the

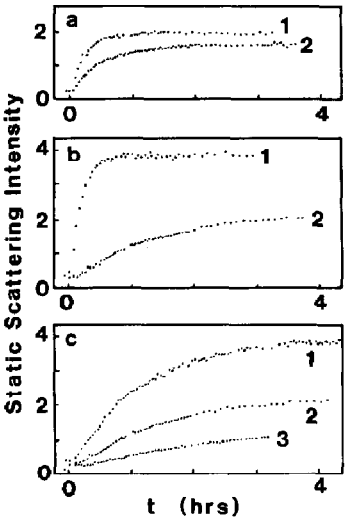


Fig. 3. Some examples of the static scattering intensities vs. time $t$ after initiation of polymerization of actin at various conditions. The scattering intensity is plotted on an arbitrary scale. Conditions were 60 mM KCl, 0.2 mM ATP, 10 mM Tris-HCl (pH 8.0) plus those below. (a) 1.0 mg/ml actin at 20°C and at 0 mM (1) and 0.2 mM (2) $CaCl_2$; (b) 2.0 mg/ml actin at 0.2 mM $CaCl_2$ and at 20°C (1) and 10°C (2); and (c) 3.0 (1), 2.0 (2) and 1.0 (3) mg/ml actin at 10°C and 0.2 mM $CaCl_2$.

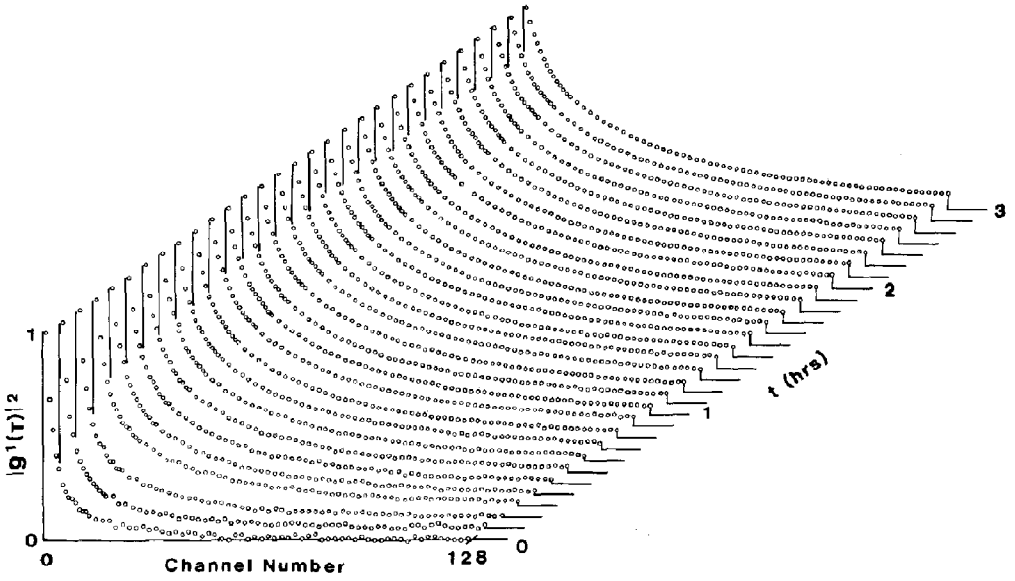


Fig. 4. Some examples showing the time evolution of the net correlation function $|g^1(\tau)|^2$ after initiation of polymerization. Conditions were 60 mM KCl, 0.2 mM ATP, 0.2 mM $CaCl_2$, 10 mM Tris-HCl (pH 8.0) and 2.0 mg/ml actin at 10°C. Scattering angle, 90°; $\Delta\tau = 20$ μs; data accumulation period 100 s/run. The $t$ (time) axis is roughly linear between 0 and 2 h. Only even channels are displayed from the 14th to the last channels.

time courses of changes in the static scattering intensities ($B^{1/2}$ in eq. 7 on an arbitrary scale) after initiation of polymerization. As shown later, the increase in the static scattering intensity reflects the progression of polymerization. Then, the results in fig. 3 show that: (a) when all conditions other than temperature are fixed, the lower the temperature, the lower is the rate of polymerization; (b) when all conditions other than the concentration of actin are fixed, the lower the actin concentration, the lower is the rate of polymerization; (c) under any condition we studied, addition of $CaCl_2$ (final 0.2 mM) with KCl lowered the rate of polymerization.

Fig. 4 depicts the time courses of changes in the net correlation functions $|g^1(\tau)|^2$ after initiation of polymerization. Changes in the initial fast decay and the evolution of a long tail in the correlation function are clearly visible. Proper analysis of the time evolution of the net correlation function will provide information about the time evolution of the sizes and the fractions of different species in the scattering cell.

### 4.3. Initial stage of polymerization of actin

We measured $G^2(\tau)$ at 5°C in order to examine the very early stage of polymerization. At low temperature, the Brownian motion also slowed down, so that $\tau_B$ increased. This allowed us to set a longer value of $\Delta\tau$ and hence to attain a larger value of $\langle n \rangle$ for a given counting rate (a given actin concentration) than those at a high temperature. However, $\langle n \rangle$ was so small at the very early stage of polymerization that the statistical accuracy in $G^2(\tau)$ for the data accumulation period of 60 s was not very high as seen in fig. 5. (A slightly lower concentration of ATP in this run may not be serious in the study of the initial stage of polymerization.) $G^2(\tau)$ values were analyzed by a two-exponential fit, and the results are shown in figs. 5 and 6. The static scattering intensity $I(t) = \langle I \rangle$ at time $t$ after initiation of polymerization can be decomposed as

$$I(t) = I_1(t) + I_2(t) \tag{10}$$

where $I_1(t) = \langle I \rangle A_1$ denotes the contribution from

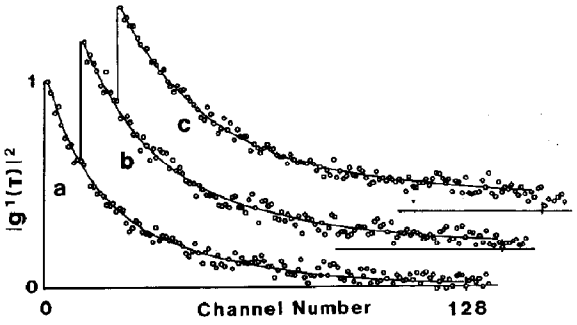


Fig. 5. Some examples of the net correlation functions $|g^1(\tau)|^2$ showing the quality of measured correlation functions and the degree of fitting in the two-exponential analysis. Conditions were 60 mM KCl, 75 μM ATP, 11 mM Tris-HCl (pH 8.0) and 1.7 mg/ml actin at 5°C. Scattering angle, 60°; $\Delta\tau = 2$ μs; data accumulation period, 60 s/run. Those after the 128th channel are some of 16 extra channels starting from $\tau = 512\ \Delta\tau$. At $t = 2$ min (a), 15 min (b) and 30 min (c).

G-actin and $I_2(t) = \langle I \rangle A_2$ from polymers (F-actin). $I(t)$ increased with $t$ after a lag phase corresponding to the nucleation process, $I_1(t)$ stayed constant and $I_2(t)$ increased after an initial lag period. Correspondingly to these changes in intensities, $D = \Gamma_1/K^2$ stayed virtually constant and $D_p = \Gamma_2/K^2$ decreased. The average value of $D = 8 \times 10^{-7}$ cm$^2$/s is close to the $D$ value of G-actin given in section 4.1. If we simply assume that $D_p$ is the average translational diffusion coefficient of polymers, we obtain the length change $L_2(t)$ of polymers as shown by open circles in fig. 6, where for conversion of $D_p$ to $L_2(t)$ use was made of Broersma's formula for the translational diffusion coefficient [15]. The two-exponential fit became poor for $t \geqq 90$ min because of the appearance of a very long tail in $G^2(\tau)$.

### 4.4. Middle and later stages of polymerization

We measured $G^2(\tau)$ at 10°C, at a slightly higher rate of polymerization than that in section 4.3. In fig. 7 are shown some of the net correlation functions $|g^1(\tau)|^2$. In this case, the two-exponential fit was very poor even for the first $G^2(\tau)$ because of a very long tail in $G^2(\tau)$ like that at the later stage in section 4.3. Then, a three-exponential fit was applied, the results being shown in figs. 7 and 8. Fig. 8a shows the time evolution of $A_i$ ($i = 1$, 2 and 3). It should be noted that soon after the initiation of polymerization the ratio $A_1 : A_2 : A_3$ became almost unity, and for $t \geqq 90$ min the ratio became constant. The static scattering intensity $I(t)$ was again decomposed as

$$I(t) = I_1(t) + I_2(t) + I_3(t) \tag{11}$$

where $I_1(t)$ and $I_2(t)$ have the same meanings as those in eq. 10 and $I_3(t) = \langle I \rangle A_3$ denotes the contribution from 'fictitious' polymers (see section 5). The rate of polymerization at 10°C was too high to observe an initial lag phase in $I(t)$, and $I(t)$ increased monotonically. $I_1(t)$ stayed constant as in section 4.3, $I_2(t)$ increased slightly and

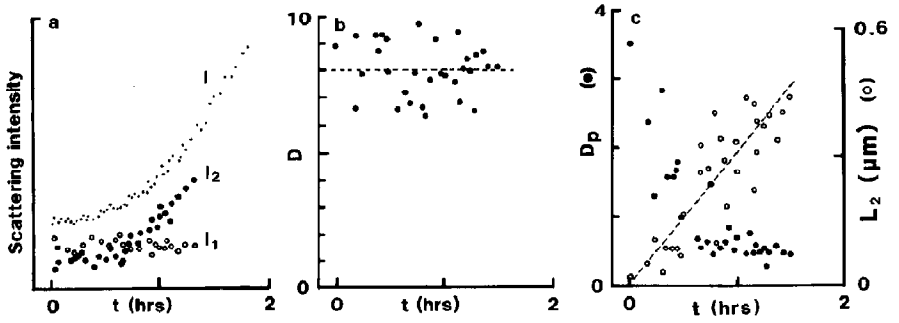


Fig. 6. Results of the two-exponential analysis of the net correlation functions $|g^1(\tau)|^2$ after initiation of polymerization. Experimental conditions were the same as those in fig. 5. (a) Static scattering intensities vs. time $t$ after initiation of polymerization (for definitions of $I$, $I_1$ and $I_2$, see text); (b) $D$ vs. $t$. $D = \Gamma_1/K^2$ in units of $10^{-7}$ cm$^2$/s at 20°C after $T/\eta$ correction; and (c) $D_p$ (●) and $L_2$ (○) vs. $t$. $D_p = \Gamma_2/K^2$ in units of $10^{-7}$ cm$^2$/s at 20°C after $T/\eta$ correction, and $L_2$ from $D_p$ by use of Broersma's formula for the translational diffusion coefficient (see text).

$I_3(t)$ increased greatly. Component 1 is considered to arise mainly from monomeric G-actin in the sample. However, the diffusion coefficient $D$ from $\Gamma_1/K^2$ of the first observed point ($t = 2$ min), $D = 3.9 \times 10^{-7}$ cm$^2$/s at 10°C or $5.3 \times 10^{-7}$ cm$^2$/s at 20°C, is much smaller than the $D$ value of G-actin obtained in section 4.1 and the $D$ value from $\Gamma_1/K^2$ obtained in section 4.3. This difference came partly from the possible coexistence of small oligomers of G-actin (e.g., $D/D^{sph} =$ 0.725 for dimer, 0.621 for triangular trimer, 0.586 for colinear trimer, etc. [16]), but mainly from the longer sampling time $\Delta\tau$ (set to be 20 $\mu$s to observe long-time behavior of $G^2(\tau)$ at the middle and later stages of polymerization) compared with those in other measurements, resulting in loss of the fast decay component to a great extent. On the other hand, the gradual decrease in $D$ values with time from the first observed point can be interpreted to be due to a slight contribution to $\Gamma_1$ from F-actin with very short lengths which appeared as a result of the size redistribution of F-actin with time (and possibly from oligomers of G-actin which might appear with time). This interpretation is also consistent with the observation that $I_1(t)$ stayed constant for a long time, up to 5 h at least, in spite of the decrease in concentration of monomeric G-actin with time. (For the size redistribution of F-actin and the concentration of monomeric G-actin at the middle and later stages, see section 5.)

Therefore, component 1 should be regarded as the contribution from actin monomers (and possibly from small oligomers and very short pieces of F-actin). If we again assume $D_p = \Gamma_2/K^2$, we obtain $L_2(t) \sim 400$ nm for $t \geqq 15$ min. At $t \sim 20$ min $A_3$ began to increase. If we tentatively assume $D_A = \Gamma_3/K^2$, the translational diffusion coefficient of the fictitious polymers, we obtain $L_3(t) \sim 2.5$ $\mu$m at $t \sim 20$ min and longer than 5 $\mu$m at $t \sim 5$ h. Although $L_3(t)$ seems to show saturation at $t \geqq 3$

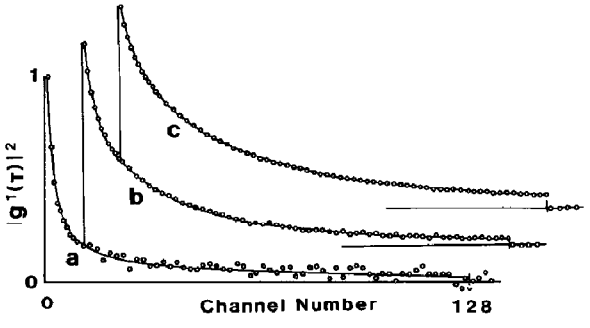


Fig. 7. Some examples of the net correlation functions $|g^1(\tau)|^2$ showing the quality of measured correlation functions and the degree of fitting in the three-exponential analysis. Conditions were 60 mM KCl, 0.2 mM ATP, 0.2 mM $CaCl_2$, 10 mM Tris-HCl (pH 8.0) and 2.0 mg/ml actin at 10°C. Scattering angle, 90°; $\Delta\tau = 20$ $\mu$s; data accumulation period, 100 s/run. At $t = 2$ min (a), 18 min (b) and 120 min (c).

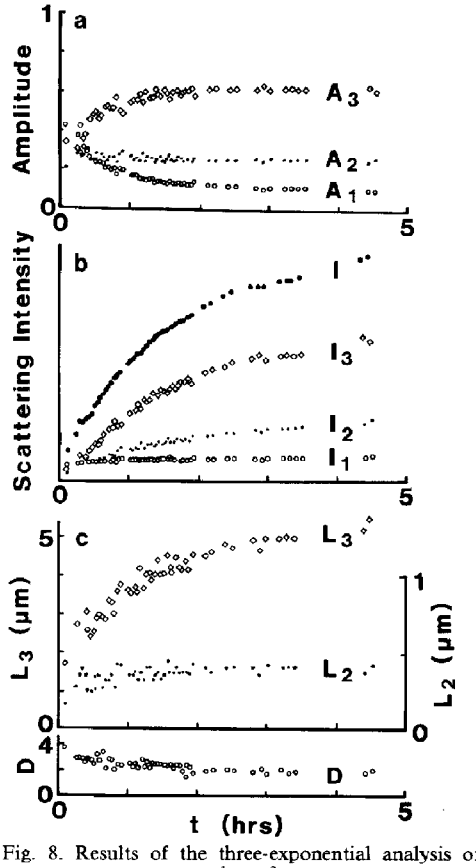


Fig. 8. Results of the three-exponential analysis of the net correlation functions $|g^1(\tau)|^2$ after initiation of polymerization. Experimental conditions were the same as those in fig. 7. (a) Amplitudes $A_i$ vs. time $t$ after initiation of polymerization; (b) static scattering intensities vs. $t$ (for definitions of $I$, $I_1$, $I_2$ and $I_3$, see text); and (c) $D$, $L_2$ and $L_3$ vs. $t$. $D = \Gamma_1/K^2$ in units of $10^{-7}$ cm$^2$/s at 10°C. $L_2$ and $L_3$ from $D_p = \Gamma_2/K^2$ and $D_A = \Gamma_3/K^2$, respectively, by use of Broersma's formula for the translational diffusion coefficient (see text).

h, this is due to the fact that the sampling time $\Delta\tau$ was kept constant (20 $\mu$s) throughout this measurement. If we lengthened the sampling time with progression of polymerization, $L_3(t)$ would show a more or less increasing behavior with time beyond $t = 3$ h.

From the experimental point of view, a good fitting of the experimental spectrum to the three-exponential function is not due simply to an increased number of unknowns to be determined but to necessity arising from the structure of the spectrum; if fitting were accidental, both $A_i$ and $\Gamma_i$ for $i = 1$, 2 and 3 might not evolve so smoothly and systematically with time as those in fig. 8. The distribution of $\Gamma_i$ in approx. 100 : 10 : 1 was indeed fortunate in the fitting. The physical rationale of the application of a three-exponential fit to a two-component system of monomers and polymers will be given at the end of section 5.

Many measurements of $G^2(\tau)$ similar to those in sections 4.3 and 4.4 were made under slightly different polymerization conditions run by run. They all gave essentially similar results to those in figs. 6 and 8.

## 5. Discussion

### 5.1. G-Actin

Our $D$ value for G-actin is very close to those from dynamic light scattering [12,13] but distinctly larger than that from fluorescence photobleaching recovery [14]. However, all of these values are consistent with the dimensions of monomeric G-actin irrespective of whether G-actin is a sphere or a prolate ellipsoid. We shall no longer discuss the $D$ value of G-actin, since our study did not concentrate on this problem and because a good account of the description of this has been given [12–14].

### 5.2. Static scattering intensity

For a system where G-actin and F-actin coexist, the static scattering intensity $\langle I \rangle$ can be written as a sum of two components; $\langle I \rangle = \langle I \rangle_G + \langle I \rangle_F$ where $\langle I \rangle_G$ is the contribution from G-actin and $\langle I \rangle_F$ from F-actin. Let $N(L)$ be the length distribution function of F-actin (the number of filaments with length in the range $L$ to $L + dL$) and $P(KL)$ be the scattering function for a thin rod with length $L$. For $KL \geqq 1$ (or $L \geqq 40$ nm for a 488 nm beam from an $Ar^+$ laser at a scattering angle of 90°), we have $P(KL) \sim (KL)^{-1}$ and $L^2N(L)P(KL) \sim LN(L)/K$. Then, the average intensity $\langle I \rangle_F$ is given by [17]

$$\langle I \rangle_F = K_{opt} C_h \tag{12}$$

where $K_{opt}$ is a proportionality constant (appendix A2). Except for the very early stage of polymerization, we can expect $\langle I \rangle_G \ll \langle I \rangle_F$, so that $I(t) = \langle I \rangle$ is approximately proportional to $C_h(t)$, the total number-concentration of G-actin incorporated into all F-actins present at time $t$ after initiation of polymerization. Then, the results in fig. 3 show the time course of the polymerization process of G-actin to F-actin. However, the information on actin polymerization provided by static light scattering is not more extensive than that obtained previously by simple viscometry (see, for example, ref. 1). On the other hand, the dynamic light-scattering technique is powerful if we can extract information about sizes and fractions of various species in the scattering cell from the time evolution of the net correlation function as shown in fig. 4.

### 5.3. The initial stage of polymerization

Experimental spectra obtained at the early stage of polymerization were decomposed into two components as shown in fig. 6. In this case, we can assume that $I_1(t) = \langle I(t) \rangle_G$ and $I_2(t) = \langle I(t) \rangle_F$ in eq. 12, because the $D$ value from $\Gamma_1/K^2$ gives a fairly good agreement with that of a monomeric actin. In spite of rather large scatter in experimental results, the behaviors of $I_2(t)$ and $L_2(t)$ in fig. 6 are consistent with the theoretical predictions shown in fig. 1; $I_2(t) \propto C_h(t)$ shows an initial lag period, and the average length $L_2(t)$ estimated from $D_p = \Gamma_2/K^2$ increases roughly linearly with $t$. Offsetting in $I_2(t)$ at the very early stage of polymerization could be attributed to artifacts in the forced two-exponential fit to net correlation functions without high statistical accuracy, be-

cause $D_p/D$ was only 1/2–1/3 for the first few points. It should be noted, however, that $D$ values stayed virtually constant even after the lag period; this is a verification of the reasonableness of the two-exponential analysis. Lanni and Ware [14] also observed a high-mobility component with $D = (7.2–7.5) \times 10^{-7}$ cm$^2$/s for KCl- and $MgCl_2$-induced polymerization and for the supernatant of a solution of actin polymerized by KCl.

Here, we have to examine the meaning of the rod length estimated from light scattering. The translational diffusion coefficient obtained by dynamic light scattering is the so-called $z$-average one, $\langle D \rangle_z$. Since the translational diffusion coefficient as a function of the rod length $L$ and rod diameter $d$ is given by $D(L) = (C/L)[\ln(2L/d) - 0.73]$ except for minor correction terms [15] where $C$ is a constant, $\langle D \rangle_z$ can approximately be given by

$$\langle D \rangle_z = (C/\langle L \rangle)[\langle \ln(2L/d) \rangle - 0.73] \sim D(\langle L \rangle) \tag{13}$$

where $\langle \ln(2L/d) \rangle \sim \ln(2\langle L \rangle/d)$ was assumed (see appendix A2 for a more exact form) and use was made of the approximation $P(KL) \sim (KL)^{-1}$ for $KL \geqq 1$ as before. The polymer length $L_2(t)$ from $\Gamma_2/K^2$ at high angles gives a rough estimate of $\langle L \rangle$, the number-average length (see appendix A2).

### 5.4. Middle and later stages of polymerization

We now discuss the results shown in fig. 8. The polymer length $L_2(t)$ was constant (about 400 nm) for $t \geqq 15$ min. This value was estimated under the assumption that $\Gamma_2$ was contributed from only translational diffusion of the rigid rod. However, we have to take account of the contribution to $\Gamma_2$ from rotational diffusion of the rigid rod as well. According to our theory for a rigid rod with length $L$, the first cumulant $\bar{\Gamma}$ is given by [18]

$$\bar{\Gamma}/K^2 = D_0 + (L^2/12)\Theta f_1(k) + (D_3 - D_1)[f_2(k) - 1/3] \tag{14}$$

where $D_0 = (2D_1 + D_3)/3$ is the overall translational diffusion coefficient, $D_1$ and $D_3$ are, respectively, the translational diffusion coefficients perpendicular to and parallel with the rod axis, $\Theta$ the end-over-end rotational diffusion coefficient, and $f_1(k)$ and $f_2(k)$ functions depending only on $k = KL/2$. In eq. 14, the second term indicates the contribution from rotational diffusion and the third term from anisotropy in translational diffusion. For $L = 400$ nm and $K = 2.42 \times 10^5$ cm$^{-1}$ (scattering angle of 90°), we have $k = KL/2 = 4.84$, $f_1(k) = 0.66$ and $f_2(k) - 1/3 = -0.26$ [18]. On the other hand, Broersma's formulas [15,19] give $D_0 = 4.29$ and $(D_3 - D_1) = 1.90$ in units of $10^{-8}$ cm$^2$/s and $\Theta = 192$ s$^{-1}$ at 20°C and $d = 8$ nm (diameter of F-actin). Then, we have $(L^2/12) \times \Theta f_1(k) = 1.69$ and $(D_3 - D_1)[f_2(k) - 1/3] = -0.49$ both in units of $10^{-8}$ cm$^2$/s, and the sum of the second and third terms in eq. 14 amounts to $1.20 \times 10^{-8}$ cm$^2$/s. To estimate the average length of F-actin from the $D$ ($D_0$) value, we have to subtract $1.20 \times 10^{-8}$ cm$^2$/s from $\Gamma_2/K^2$, which results in the new $L$ value of 560 nm. For $L = 560$ nm, we reevaluate eq. 14 and obtain $\bar{\Gamma}/K^2 = (3.34 + 1.49 - 0.45) \times 10^{-8}$ cm$^2$/s $= 4.38 \times 10^{-8}$ cm$^2$/s, which should be compared with $D_0 = 4.29 \times 10^{-8}$ cm$^2$/s given just above for $L = 400$ nm. For a semiflexible and long rod such as F-actin, we have then to take into account the effect of flexibility of the rod on the transport coefficients $D_i$ ($i = 0$, 1 and 3) and $\Theta$. For example, we have $D_0$(semiflexible) $= 3.57 \times 10^{-8}$ cm$^2$/s and $D_0$(rigid rod) $= 3.34 \times 10^{-8}$ cm$^2$/s for $L = 560$ nm and $\gamma = 0.2$ $\mu$m$^{-1}$ (flexibility parameter, see appendix A3). From $D_0$(semiflexible) $= 3.34 \times 10^{-8}$ cm$^2$/s (rigid-rod value for $L = 560$ nm) we have $L = 600$ nm. In addition to these, we have to take account of the contribution to $\bar{\Gamma}/K^2$ (or $\Gamma_2/K^2$) from the flexion motion of the semiflexible rod. As detailed in appendix A3, $L_2(t) = 400$ nm estimated from $\Gamma_2/K^2$ should read $L_2(t) = 900$ nm, namely, the expected number-average length of F-actin at $t \geqq 15$ min is about 900 nm. Since component 1 in the three-exponential fit can be identified as being the contribution from actin monomers, we can put $\langle I \rangle_G = I_1(t)$ and $\langle I \rangle_F = I_2(t) + I_3(t)$. The intensity $I$(20 min) at $t = 20$ min was about one-fifth of $I$(24 h), the intensity at $t = 24$ h when all the polymerization processes were considered to finish. Then, we can expect $\langle I(20 \text{ min}) \rangle_F / \langle I(24 \text{ h}) \rangle_F \sim 1/5$. (It should be noted that at $t = 20$ min $C_h/C_0$

$= 1/5$ and hence the nucleation process almost finished, $p(t)/p(\infty) \sim 0.8$.) From eq. 12, the concentration of F-actin (or the total concentration of G-actin incorporated into all polymers) is estimated to be about 0.4 mg/ml, because the initial G-actin concentration in this case was 2.0 mg/ml. A length of $L = 900$ nm and a concentration of polymers of $C_p = 0.4$ mg/ml give $pL^3 \sim 10$, a condition just entering a semidilute region, where $p$ denotes the number concentration of polymers as before. In such a situation as $pL^3 \gg 1$ (semidilute regime), $G^2(\tau)$ exhibits a very long tail [10]. The long tail arises from a restricted motion of long filaments in a semidilute solution and not from fictitious polymers (for some comments, see below). The onset of the increase in $I_3(t)$ coincides with the onset of a semidilute regime. Then, the increases in $I_3(t)$ and $L_3(t)$ with $t$ correspond to the increasing contribution to the dynamic light-scattering spectrum from the restricted motion. The increase in $pL^3$ with $t$ will occur if the average length $\langle L(t) \rangle$ increases with $t$ keeping $p(t)$ constant as depicted in fig. 1. This interpretation, however, is in contradiction to the fact that $L_2(t)$ stayed constant, and furthermore, $pL^3$ increases too rapidly. Another possible and simple interpretation is provided by assuming spontaneous fragmentation of F-actin. In this case, $p$ increases on fragmentation and association of G-actin to fragmented F-actin recovers the length, resulting in a gradual increase in $p(t)$, keeping the average length over all filaments constant. This process is possible: from $\langle I(90 \text{ min}) \rangle_F / \langle I(24 \text{ h}) \rangle_F \sim 1/2$, we can estimate a monomeric G-actin concentration of 1 mg/ml at $t = 90$ min. Since each F-actin with length 900 nm has 360 incorporated G-actins, the monomer concentration $C_1(t)$ in the solution is 360-times higher than the polymer concentration $p(t)$ at $t = 90$ min. This fragmentation-elongation process is also expected to be a major mechanism of size redistribution of F-actin from a Poisson-type distribution to the final exponential-type distribution (see section 5.5 below).

Our interpretation given above is quite consistent with the following observation [20]. Under a condition that 18 hours were required for the full process of polymerization of actin, electron microscopic observations showed that the length distribution was Poissonian for $t \leqq 5$ min and exponential for $t \geqq 20$ min. $C_h(t)$ was about 10% of the initial G-actin concentration at $t = 20$ min and about 80% at t = 3 hours. The number-average length was constant (about 880 nm) for $t \geqq 20$ min.

### 5.5. Some remarks

#### 5.5.1. Fragmentation

We introduced the fragmentation-elongation process to understand the time-evolution behavior of the net correlation function. The importance of this process in actin polymerization (which was briefly discussed in ref. 1 but not included in the original Oosawa-Kasai theory [5]) was explicitly discussed by Wegner [21] and Wegner and Savko [22]. Several papers then appeared, including one for Ca-actin in the $K^+$-induced polymerization [23] and another for Mg-actin in the $Mg^{2+}$-induced polymerization [24].

#### 5.5.2. Size redistribution

Tail-to-head association (or reannealing [24]) of (fragmented) actin filaments would result in size redistribution as well, but this process is most unlikely compared with the fragmentation-elongation process not only because of the concentration relationship $C_1 \gg p$ in the middle stage of polymerization but also because of the low probability of a tail-to-head collision of two filaments in the proper coordination for reannealing compared with the probability of a collision of G-actin with the growing end of (fragmented) F-actin [25]. Indeed, under controlled fragmentation by sonication, this tail-to-head association was suggested not to be dominant [26]. At the latest stage of polymerization where the concentration $C_1$ becomes very low, however, the fragmentation-elongation process with the backward reaction would work at the cost of a very long time (in a random-walk way [26]) to attain the truly equilibrium length distribution of F-actin as first suggested in ref. 27.

If we can measure the intensity correlation function in the delay time of not equal but variously arranged spacing, we can obtain information

about the fast and very slow decay components at the same time even with a limited number of channels of the correlator. By using such correlation functions, we can, in principle, analyze the time evolution of the size distribution and possibly the size redistribution of the scatterers in the sample. The present result suggests the feasibility of such studies, although there are many problems to be overcome; technical problems include low $\langle n \rangle$ values at the initial stage of polymerization and theoretical problems include effects of the flexibility and restricted motion of filaments on the spectrum at the middle and later stages of polymerization.

*5.5.3. Fictitious polymers*

We again discuss fictitious polymers whose length $L_3(t)$ was estimated from $D_A = \Gamma_3/K^2$. From fig. 8, we observe $L_3(5\ \text{h}) = 5\ \mu\text{m}$. This length, if this is the true one, should be the number-average length as eq. 13 shows. If we take account of the effects on $\Gamma_3$ of rotational and bending motions of such a long filament, as discussed above for $\Gamma_2$, the reestimated length would be longer than 15 $\mu$m in the number-average length. According to electron-microscopic observations, the longest filament in various preparations always shows a length greater than 5 $\mu$m, but the number-average length over all observed filaments never exceeds 2 $\mu$m under the usual polymerization conditions as in the present one, and especially for an initial actin concentration of 2 mg/ml as in our case, the number-average length was 880 nm and the longest one in the exponential distribution was 6.7 $\mu$m as late as $t = 3$ days [20]. The fictitious polymer is not a real entity undergoing free Brownian motion, and it should be regarded as a dynamic light-scattering 'ghost' due to the restricted motion of filaments in a semidilute solution as mentioned above. What kind of a restricted motion is expected? In the case of monodisperse filaments such as bacteriophage fd, the very slow component(s) indeed appears in a semidilute regime, but its fraction is not large even at $pL^3 = 75$ (see fig. 8 in ref. 28). For a semidilute solution of very long filaments with uniform length, the diameter of the cage which confines the motion of filaments is comparable to or larger than $1/K$ except for small $K$. Such a situation is quite different from the situation assumed in the model of Doi-Edwards [29], for example. In the case of polydisperse F-actin, on the other hand, the very slow component(s) appears with a large fraction even at $pL^3 \sim 10$ and at $K^2 = 0.9 \times 10^{10}$ cm$^{-2}$ (or a scattering angle of 32°) [10]. Our observation over a range of scattering angles from 30 to 130° suggests that such a very slow component(s) in the spectrum from in vitro reconstituted F-actin is due to a reptile motion of very long filaments, which form the far tail of an exponential length distribution, in the cages formed by filaments with lengths around the number-average length $\langle L \rangle$ (Fujime et al., unpublished results). Although the number of such very long filaments is small, their contribution to the spectrum may be large as inferred from our simulation of $\langle D \rangle_z$ in appendix A2. Increasing of component 3 is concluded to be due to an increase in the number of filaments much longer than the average length, which comes from the size redistribution of F-actin from a Poisson type to an exponential type through the fragmentation-elongation process. The major fraction of filaments would undergo almost free Brownian motion even for $p\langle L \rangle^3 > 10$ as does monodisperse fd.

*5.5.4. Three-exponential fit*

During the polymerization process of actin, the scatterers are classified roughly into two species, monomers (and possibly its small oligomers) and polymers (with a broad length distribution). Thus, it is quite natural to adopt the two-exponential fit of the field correlation function. Why the three-exponential fit in the middle and later stages of polymerization? We first tried to fit the experimental function to a two-exponential decay. Then, we observed not only a very poor fitting but also a long length $L_2(t)$, which was nearly equal to the length $L_2$ from $\Gamma_2 = (A_2\Gamma_2 + A_3\Gamma_3)/(A_2 + A_3)$ in the three-exponential fit. Such a long length of polymers was hard to accept on the basis of electron microscopic observations [20] and of an estimated value of $pL^3 \ggg 1$. Although species in the scattering cell are monomers and polymers, there are three components in the scattering spectrum: those due to free Brownian motion of

monomers, almost free Brownian motion of polymers with a number-average length of 900 nm and restricted motion of very long polymers mentioned above. Our previous study using F-actin with the final length distribution ($t > 3$ days) showed that the transition from the dilute to semidilute regime occurred at about 0.3 mg/ml F-actin [10]. It is thus very likely that the onset of the semidilute region appeared at $t \sim 80$ min in fig. 6 and at $t \sim 20$ min in fig. 8.

If we tentatively assume that component 3 arises from freely moving scatterers, our result is quite compatible with the result of Lanni and Ware [14] by fluorescence photobleaching recovery. They obtained a length of low-mobility species longer than 10 $\mu$m in the same way as we have done for obtaining $L_3$ from $D_A$. However, we do not believe that the very slowly decaying component in the dynamic light-scattering spectrum from F-actin was due to free motions of such long filaments. Because the mechanism producing the spectrum and the preparation of G-actin in our study are different from those in [14], our conclusion does not necessarily deny their interpretation about low-mobility species.

## 6. Conclusions

By the dynamic light-scattering technique, we obtained: (1) The translational diffusion coefficient of G-actin is $(8.07 \pm 0.10) \times 10^{-7}$ cm$^2$/s at 20°C. This value is consistent with the dimensions of monomeric G-actin. (2) During the polymerization of actin, the fast component of the intensity correlation functions always comes from G-actin (and possibly its small oligomers), the slow component arising from growing F-actin whose number-average length increased linearly with time at the early stage of, and stayed constant at the middle and later stages of polymerization. (3) The slowest component appearing in the middle and later stages of polymerization is concluded to come from the restricted motion of very long F-actin in a semidilute regime. (4) From the growing process of the last component, we deduce that the fragmentation-elongation process starts to occur as early as the middle stage when $\langle I(t)\rangle_F / \langle I(\infty)\rangle_F \sim 1/5$, which results in the size redistribution of F-actin. (5) The $z$-average diffusion coefficient $\langle D\rangle_z$ is given by an 'adapted' Broersma formula, $D(L, \alpha)$ in eq. A6, with $L = L_w$ for $KL = 0$ and $L = L_n$ for $KL \geqq 1$, where $\alpha$ depends on the polydispersity parameter $\nu$. (6) Dynamic light scattering can be applied to the study of quasistationary processes without any labeling as in fluorescence methods, when the time evolution of the system in question is moderately slow. Although the present study is not sufficiently complete for the analysis of the polymerization process of actin, it does demonstrate the feasibility of this kind of study.

## Appendix

### *A1. Multiexponential analysis*

We briefly describe our algorithm of a multiexponential analysis. For a two-exponential analysis, an integration method [30] was adopted to obtain approximate values of $\Gamma_i$ and $A_i$ for $i = 1$ and 2. Next, these values were refined by a linearized iteration method, i.e., $(A_i + \delta A_i)\exp[-(\Gamma_i + \delta\Gamma_i)\tau] \sim A_i\exp(-\Gamma_i\tau) + \exp(-\Gamma_i\tau)\delta A_i - \tau A_i \times \exp(-\Gamma_i\tau)\delta\Gamma_i$. For a three-exponential analysis, the results of the integration method were used as the initial values of $\Gamma_i$ and $A_i$ for $i = 2$ and 3, and $\Gamma_1 = 2.5 \times 10^5$ s$^{-1}$ (for the case in fig. 8) and $A_1 = 0$ were arbitrarily assumed. These values were refined by a linearized iteration method where $\Gamma_1$ was fixed. The results of this five-parameter iteration method were further refined by a six-parameter linearized iteration method. Four to five cycles of iteration were enough to satisfy the convergence conditions $|\delta X_i|/(X_i + \delta X_i) \leqq 0.001$ for $X_i = A_i$ and $\Gamma_i$ with $i = 1$, 2 and 3.

### *A2. On the translational diffusion coefficient averaged over length distribution*

Here, we discuss $\langle D\rangle_z$ defined by eq. A1 quantitatively.

$$\langle D\rangle_z = \int D(L)L^2N(L)P(KL)\mathrm{d}L \Big/ \int L^2N(L)P(KL)\mathrm{d}L \qquad \text{(A1)}$$

For simplicity, we assume the Schulz-Zimm distribution function [31];

$$N(L)\,dL = N_r z^{\nu} \exp[-(\nu+1)z]\,dz \quad (z = L/L_n) \tag{A2}$$

where $N_r$ is the normalization constant, $\nu$ the distribution parameter and $L_n$ the number-average length ($= \langle L \rangle$ in the text). This distribution gives the exponential distribution for $\nu = 0$; the larger the $\nu$ value, the sharper the distribution. Eq. A2 gives the weight-average length $L_w$ as

$$L_w = \int L^2 N(L)\,dL / \int LN(L)\,dL = [(\nu+2)/(\nu+1)]\,L_n \tag{A3}$$

To evaluate eq. A1 with A2 and $D(L) = (k_B T/3\pi\eta L)[\ln(2L/d) - 0.73]$, we use the following formulas for any $\nu$ with a positive real part [32]:

$$\Gamma(\nu) = \int e^{-z} z^{\nu-1}\,dz \quad \text{(gamma function)}$$

$$\Gamma'(\nu) = d\Gamma(\nu)/d\nu = \int e^{-z} z^{\nu-1} \ln(z)\,dz$$

$$\psi(\nu) = \Gamma'(\nu)/\Gamma(\nu) = \sum_n (1/n) - \gamma \quad \text{(di-gamma function)}$$

where the integration range is $[0, \infty]$, $n$ in the summation runs from 1 to $(\nu - 1)$ and $\gamma$ is Euler's constant ($= 0.57721\ldots$).

*A2.1. In the limit of $K = 0$*

In this limit, we have $P(KL) = 1$ and

$$\langle D \rangle_z^o = D_w(L_w) = (k_B T/3\pi\eta L_w) \times [\ln(2\alpha L_n/d) - 0.73] \tag{A4}$$

with

$$\ln(\alpha) = \psi(\nu+2) - \ln(\nu+1)$$

where the superscript o denotes a quantity at $K = 0$ and use was made of an identity relation $\ln(2L/d) = \ln(L/L_n) + \ln(2L_n/d)$. The numerical values of $\alpha$ are 1.53 ($\nu = 0$), 1.13 ($\nu = 3$) and 1.05 ($\nu = 10$), for example; $\alpha L_n < L_w$.

*A2.2. For $KL \geqq 1$*

In this range of $KL$ values, we have $P(KL) \sim (KL)^{-1}$ and

$$\langle D \rangle_z = D_n(L_n) = (k_B T/3\pi\eta L_n) \times [\ln(2\alpha' L_n/d) - 0.73] \tag{A5}$$

with

$$\ln(\alpha') = \psi(\nu+1) - \ln(\nu+1)$$

The numerical values of $\alpha'$ are 0.56 ($\nu = 0$), 0.88 ($\nu = 3$) and $0.95_5$ ($\nu = 10$), for example; $\alpha L_n < L_n$.

*A2.3. Numerical examples*

Now, we compute $\langle D \rangle_z$ given by eq. A1 with eq. A2 and Broersma's formula for $D(L)$ including minor terms due to end effects. The integration in eq. A1 was replaced with the summation up to $L = 6000$ and 600 nm with steps of $\Delta L = 50$ and 5 nm for $L_n = 900$ and 90 nm, respectively. Numerical evaluation of $P(KL)$ can easily be made according to the algorithm in ref. 33. The numerical results for the profiles of $N(L)$ are shown in fig. 9a, for the $\langle D \rangle_z$ vs. $K^2$ relationships in fig. 9b ($L_n = 900$ nm and $d = 8$ nm) and in fig. 9c ($L_n = 90$ nm and $d = 2$ nm). The broken lines in fig. 9b and c show the values of $D(L_n, 1)$, the Broersma value of $D$ for $L = L_n$, where $D(L, \alpha)$ is defined by

$$D(L, \alpha) = (k_B T/3\pi\eta L) \times [\ln(2\alpha L_n/d) - f(2\alpha L_n/d)] \tag{A6}$$

with

$$f(x) = 0.73 - 2.1(x^{-1} - 0.39)^2 - 3.7(x^{-1} - 0.34)^2$$

which is the same as Broersma's formula for $\alpha L_n = L$, as eq. A4 for $f(x) = 0.73$ and as eq. A5 for $\alpha'$ and $f(x) = 0.73$.

We first discuss the results for $L_n = 900$ nm (very long rods). In this paragraph, $D$ values are given in units of $10^{-8}$ cm$^2$/s and $K^2$ in units of $10^{10}$ cm$^{-2}$. For $\nu = 0$, $\langle D \rangle_z$ starts from 1.27 at $K^2 = 0$, very rapidly increases in a very low $K^2$ region and shows saturation at high $K^2$ (2.02 at $K^2 = 9$). For $\nu = 3$, $\langle D \rangle_z$ starts from 1.90 at $K^2 = 0$, again rapidly increases in a very low $K^2$ region and approaches $D(L_n, 1)$. Table 1 lists $D$ values at $K^2 = 0$ and 9. For an exponential distribution

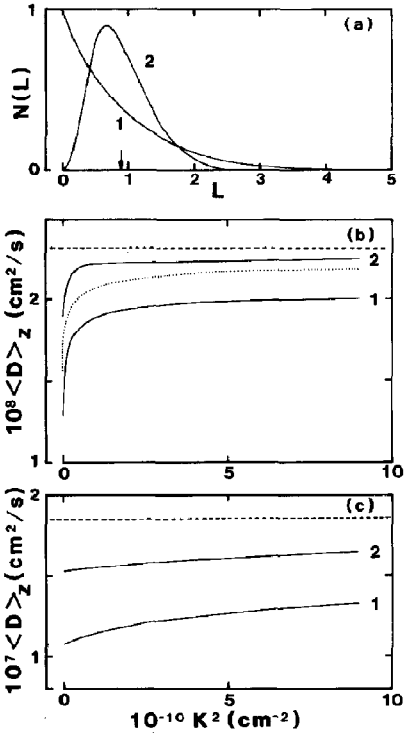


Fig. 9. Numerical simulation of the $z$-average translational diffusion coefficient $\langle D \rangle_z$ at 20°C for a Schulz-Zimm distribution function $N(L)$. In (a–c), solid lines 1 for $\nu = 0$ and solid lines 2 for $\nu = 3$. (a) Profiles of $N(L)$. The arrow shows the location of $L_n$. (b) $\langle D \rangle_z$ for $L_n = 900$ nm, $d = 8$ nm. The dotted line was computed by truncating $N(L)$ for $\nu = 0$ at $L = 3000$ nm. (c) $\langle D \rangle_z$ for $L_n = 90$ nm, $d = 2$ nm. In (b and c), broken lines show the Broersma values of $D$ for $L = L_n$.

($\nu = 0$), $D(L_n, 1)$ is not a very good approximation of $\langle D \rangle_z$ at high $K^2$ of long rods, but it is much better than $D(L_w, L_w/L_n)$, the Broersma value for $L = L_w$. For such a small $\nu$ value as 3, on the other hand, $D(L_n, 1)$ is a fairly good approximation of $\langle D \rangle_z$ at high $K^2$. It should be noted that except for a low $K^2$ region, $\langle D \rangle_z$ shows a plateau value which is much closer to $D(L_n, \alpha')$ and even closer to $D(L_n, 1)$ than to both $D(L_w, \alpha)$ and $D(L_w, L_w/L_n)$. This feature arises solely from the very longness of scatterers; an approximation of $P(KL) \sim (KL)^{-1}$ holds for a major fraction of scatterers except for very low $K^2$.

We next discuss the results for $L_n = 90$ nm (relatively short rods). In this paragraph, $D$ values are given in units of $10^{-7}$ cm²/s. For $\nu = 0$ (3), $\langle D \rangle_z$ starts from 1.09 (1.53) at $K^2 = 0$ and gradually increases with $K^2$, but $\langle D \rangle_z$ values in an experimentally accessible range of $K^2$ are much closer to $D(L_w, L_w/L_n)$ than to $D(L_n, 1)$ (broken line in fig. 9c).

It is generally concluded that the light-scattering process weights effects of long filaments much more heavily than short filaments. This is true for $KL < 1$ or at very low $K^2$. Due to this, $\langle D \rangle_z$ values at $K^2 = 0$ are very small (fig. 9b). Note the much smaller value of $\langle D \rangle_z$ at $K^2 = 0$ for $\nu = 0$ than that for $\nu = 3$. As $K^2$ increases, on the other hand, a lesser contribution of long filaments than short ones results in a rapid increase in $\langle D \rangle_z$. However, the contribution to $\langle D \rangle_z$ from long filaments is still significant as shown by the dotted line in fig. 9b, which was computed by truncating $N(L)$ for $\nu = 0$ at $L = 3000$ nm. In our particular example of a three-exponential analysis given in the text, very short pieces of F-actin would contribute to the first component $A_1$, very long filaments to the third component $A_3$, and the filaments with a broad (low $\nu$) length distribution centered around $L_n$ to the second component $A_2$.

The same situation as above also appears in the

Table 1

List of $D$ values in units of $10^{-8}$ cm²/s computed for $L_n = 900$ nm, $d = 8$ nm and 20°C

$\langle D \rangle_z$ was obtained from numerical integration of eq. A1, $D_w(L_w)$ from eq. A4, $D_n(L_n)$ from eq. A5 and $D(L, \alpha)$ from eq. A6. $\alpha^* = L_w/L_n$. $D(L_w, \alpha^*)$ and $D(L_n, 1)$ are the Broersma values for $L = L_w$ and $L = L_n$, respectively.

| $\nu$ | $K^2 = 0$ | | | | $K^2 = 9\times10^{10}$ cm$^{-2}$ | | | |
|---|---|---|---|---|---|---|---|---|
| | $\langle D \rangle_z$ | $D_w(L_w)$ | $D(L_w, \alpha)$ | $D(L_w, \alpha^*)$ | $\langle D \rangle_z$ | $D_n(L_n)$ | $D(L_n, \alpha')$ | $D(L_n, 1)$ |
| 0 | 1.27 | 1.23 | 1.27 | 1.34 | 2.02 | 1.97 | 2.02 | 2.32 |
| 3 | 1.90 | 1.85 | 1.90 | 1.95 | 2.24 | 2.19 | 2.25 | 2.32 |

derivation of eq. 12:

$$\langle I\rangle_F = C'\int L^2P(KL)N(L)\,dL/\int N(L)\,dL$$
$$= C'L_wL_n \quad (KL\to 0)$$
$$= C'L_n/K \quad (KL\geqq 1)$$

where $C'$ is a proportionality constant. Let $L_o$, $\langle i\rangle$ and $p$ be, respectively, the unit length, average degree of polymerization and number of polymers. Then, we have $L_n = L_o\langle i\rangle$ and $C_h = \langle i\rangle p$, and hence $\langle I\rangle_F = C'L_n/K = K_{opt}C_h$ at high $K$ as in eq. 12. For $KL\to 0$ (short $L$ and/or low $K$), on the other hand, $\langle I\rangle_F$ is proportional to $C_h^2$.

### *A3. Estimation of filament length*

For a semiflexible and long rod, we have instead of eq. 14

$$\bar{\Gamma}/K^2 = D_0 + (L^2/12)\Theta f_1^*(k) + (D_3 - D_1)$$
$$\times[f_2^*(k) - 1/3]$$
$$+ (k_BT/4\pi\eta L)\sum_m (1+f_m)a_m(k) \quad (A7)$$

where $f_i^*(k)$ $(i=1,\ 2)$ and $a_m(k)$ $(m\geqq 2)$ are functions depending on both $k$ and the flexibility of the rod, and $f_m$ $(m\geqq 2)$ denotes the hydrodynamic interaction factor [34] so that $D_{[m]} = (k_BT/4\pi\eta L)(1+f_m)$ is the diffusion coefficient of the $m$-th mode $(m\geqq 2)$ of the internal bending motion. In the stiff limit, $f_1^*(k)$ and $f_2^*(k)$ tend toward $f_1(k)$ and $f_2(k)$ for the rigid rod, respectively, and $a_m(k)$ toward zero. Explicit expressions for $f_i^*(k)$ for $i=1$ and 2, and $f_m$ and $a_m(k)$ for $m\geqq 2$ can be found elsewhere [34–36]. In our notation, the mode number $m$ is assigned as 0 for translation, 1 for rotation, 2 for the lowest bending mode, etc. The first term in eq. A7 shows the contribution from translational diffusion, the second from rotational diffusion, the third from anisotropy in translational diffusion, and the fourth term(s) from bending motion(s). In eq. A7, transport coefficients $D_i$ $(i=0,\ 1$ and $3)$ and $\Theta$ are functions of $L$, $d$ and $\gamma$ (the flexibility parameter or the inverse of the Kuhn length);

$$D_i(\text{semiflexible}) = D_i(\text{rigid rod})g_{t,i}(L,\ d,\ \gamma)$$
$$(i=0,1,3) \quad (A8)$$

$$\Theta(\text{semiflexible}) = \Theta(\text{rigid rod})g_{rot}(L,\ d,\ \gamma) \quad (A9)$$

where $D_i$(rigid rod) and $\Theta$(rigid rod) are given in refs. 15 and 19, the functions $g_{t,0}(L,\ d,\ \gamma)$ in ref. 37, $g_{rot}(L,\ d,\ \gamma)$ in refs. 38 and 39 and $[D_3(\text{semiflexible}) - D_1(\text{semiflexible})]/D_0(\text{semiflexible})$ in ref. 40.

Computation of numerical values of $f_i^*(k)$ for $i=1$ and 2 and $a_m(k)$ for $m\geqq 2$ involves 3-fold integration, which was carried out by using an adaptive multidimensional quadrature subroutine, ADAPT [28], on a minicomputer (Eclipse S-140, Nippon Data General, Tokyo). The algorithm for the present computation has been outlined in ref. 36.

The analysis based on eq. A7 has a difficulty; how many modes in eq. A7 should be taken into account? There are two simple criteria: the relaxation time $\tau_m$ of the $m$-th mode should be longer than the sampling time $\Delta\tau$; the mean-square-amplitude $\langle\delta_m^2\rangle$ $(=2D_{[m]}\tau_m)$ of the $m$-th mode should not be much smaller than $1/K^2$. These two criteria are too qualitative and not enough to determine unequivocally the number of modes to be included. Then, before discussing the result for F-actin, we would like to refer to the result for a dilute suspension of monodisperse filamentous bacteriophage fd, because this gives a good guide to the present analysis. This phage is 895 nm long and 9 nm thick. The experimental value of $\bar{\Gamma}/K^2$ for this phage was $4.45\times 10^{-8}$ cm$^2$/s at 20°C and a scattering angle of 90°. Our analysis based not on eq. A7 but on a direct method gave $\gamma = 0.26$ $\mu$m$^{-1}$ [28]. On the other hand, eq. A7 can estimate $\bar{\Gamma}/K^2$ as

$$\bar{\Gamma}/K^2 = 2.41 + 1.21 - 0.27 + 0.66 \quad (m=2)$$
$$+ 0.62 \quad (m=3)$$

in units of $10^{-8}$ cm$^2$/s. Thus, we have $\bar{\Gamma}/K^2 = 4.01\times 10^{-8}$ cm$^2$/s for $m$ up to 2 and $4.63\times 10^{-8}$ cm$^2$/s for $m$ up to 3. The full contribution to $\bar{\Gamma}/K^2$ from the $m=2$ mode and a partial contribution from the $m=3$ mode in this particular case are consistent with the two criteria above; $\tau_2 = 1300$ $\mu$s, $\tau_3 = 180$ $\mu$s, $\langle\delta_2^2\rangle = (39\text{ nm})^2$ and $\langle\delta_3^2\rangle = (14\text{ nm})^2$, which should be compared with $\Delta\tau = 20$

$\mu$s and $1/K = 40$ nm at a scattering angle of 90° and at 20°C.

The $\gamma$ value of F-actin is not known exactly. From various measurements by different techniques, we assume here $\gamma = 0.2\ \mu m^{-1}$ for in vitro reconstituted F-actin [1,41]. We then have in units of $10^{-8}\ cm^2/s$

$$\bar{\Gamma}/K^2 = 3.38 + 1.52 - 0.42 = 4.48$$
for $L = 600$ nm
$$= 2.70 + 1.30 - 0.32 + 0.70 = 4.38$$
for $L = 800$ nm
$$= 2.25 + 1.16 - 0.26 + 0.60\ (= 3.75) + 0.56 = 4.31$$
for $L = 1000$ nm

These estimates are for a monodisperse preparation. Since, however, the effects of polydispersity on the second and third terms in eq. A7 almost cancel each out other and eq. 13 roughly holds for the first term, an increase in $\bar{\Gamma}/K^2$ due to polydispersity may not be large, if we put $L = L_n$. Then, comparing these results with $\Gamma_2/K^2 = 4.3 \times 10^{-8}$ $cm^2/s$, we can have $L_2(t) \sim 900$ nm as the best estimate of the length of F-actin at the middle and later stages of polymerization.

The above estimation of the polymer length $L_2(t)$ is based on the theoretical result for a dilute suspension of semiflexible filaments. This seems to conflict with our interpretation of component 3 in the three-exponential analysis. However, this is not so (see section 5.5.3).

**Acknowledgements**

We thank Dr. T. Maeda for his advice on the use of his subroutine ADAPT. The assistance of Mrs. M. Takasaki-Ohsita was very helpful in machine computation in the Appendix and the drawing of figures. One of us (J.M. ) acknowledges with thanks a postdoctoral fellowship (July 1982 to September 1984) from this Institute.

## References

1 F. Oosawa and S. Asakura, Thermodynamics of the polymerization of protein (Academic Press, New York, 1975).
2 C. Frieden, Annu. Rev. Biophys. Biophys. Chem. 14 (1985) 189.
3 B. Chu, Laser light scattering (Academic Press, New York, 1974).
4 B. Berne and R. Pecora, Dynamic light scattering (Interscience, New York, 1975).
5 F. Oosawa and M. Kasai, J. Mol. Biol. 4 (1962) 10.
6 H.Z. Cummins, in: The application of laser light scattering to the study of biological motion, eds. J.C. Earnshaw and M.W. Steer (Plenum, Press, New York, 1983) p. 171.
7 F.B. Straub, Stud. Inst. Med. Chem. Univ. Szeged 3 (1943) 23.
8 S. Ebashi and K. Maruyama, J. Biochem. (Tokyo) 58 (1965) 20.
9 J.A. Spudich and S.J. Watt, J. Biol. Chem. 246 (1971) 4866.
10 S. Fujime, S. Ishiwata and T. Maeda, Biophys. Chem. 20 (1984) 1.
11 D.E. Koppel, J. Chem. Phys. 57 (1972) 4814.
12 C. Montague, K.W. Lee and F.D. Carlson, J. Muscle Res. Cell Motility 4 (1983) 95.
13 J. Newman, J.E. Estes, L.A. Selden and C. Gershman, Biochemistry 24 (1985) 1538.
14 F. Lanni and B. Ware, Biophys. J. 46 (1984) 97.
15 S. Broersma, J. Chem. Phys. 32 (1960) 1632.
16 J. Garcia de la Torre in: Molecular electro-optics, ed. S. Krause, (Plenum Press, New York, 1981) p. 75.
17 E.F. Casassa, J. Chem. Phys. 23 (1955) 596.
18 T. Maeda and S. Fujime, Macromolecules 17 (1984) 1157.
19 S. Broersma, J. Chem. Phys. 32 (1960) 1620.
20 M. Kawamura and K. Maruyama, J. Biochem. (Tokyo) 67 (1970) 437.
21 A. Wegner, Nature 296 (1982) 266.
22 A. Wegner and P. Savko, Biochemistry 21 (1982) 1909.
23 J.A. Cooper, E.L. Buhle, Jr, S.B. Walker, T.Y. Tsong and T.D. Pollard, Biochemistry 22 (1983) 2193.
24 C. Frieden and D.W. Goddette, Biochemistry 22 (1983) 5836.
25 H. Kondo and S. Ishiwata, J. Biochem. (Tokyo) 79 (1976) 159.
26 M.F. Carlier, D. Pantaloni and E. Korn, J. Biol. Chem. 259 (1984) 9983.
27 F. Oosawa, J. Theor. Biol. 27 (1970) 69.
28 T. Maeda and S. Fujime, Macromolecules 18 (1985) 2430.
29 M. Doi and S.F. Edwards, J. Chem. Soc., Faraday Trans. II 74 (1978) 560.
30 S.P. Lee and B. Chu, Appl. Phys. Lett. 24 (1974) 261.
31 B.H. Zimm, J. Chem. Phys. 16 (1948) 1099.
32 M. Abramowitz and I.A. Stegun, Handbook of mathematical functions with formulas, graphs and mathematical tables, 9th edn. (Dover Publications, New York, 1970).
33 S. Fujime and K. Kubota, Biophys. Chem. 23 (1985) 1.
34 S. Fujime and T. Maeda, Macromolecules 18 (1985) 191.
35 T. Maeda and S. Fujime, Macromolecules 17 (1984) 2381.
36 K. Kubota, Y. Tominaga and S. Fujime, Macromolecules 19 (1986) 1604.
37 H. Yamakawa and M. Fujii, Macromolecules 6 (1973) 407.
38 P.J. Hagerman and B.H. Zimm, Biopolymers 20 (1981) 1481.
39 T. Yoshizaki and H. Yamakawa, J. Chem. Phys. 81 (1984) 982.
40 M. Schmidt and W.H. Stockmayer, Macromolecules 17 (1984) 509.
41 S. Fujime, in: Optical studies of muscle cross-bridges, eds. R.J. Baskin and Y. Yeh (CRC Press, Florida, 1987), in the press.